Applied Clay Science 132–133 (2016) 133–139

Contents lists available at ScienceDirect

Applied Clay Science

journal homepage: www.elsevier.com/locate/clay

Research paper

Silylation of saponite with 3-aminopropyltriethoxysilane

Qi Tao [a,b,c,*], Yan Fang [a,c,d], Tian Li [e], Dan Zhang [a,c,d], Manyou Chen [a,c,d], Shichao Ji [a,c,d], Hongping He [a,c,d], Sridhar Komarneni [b,*], Huaibin Zhang [b], Yan Dong [b], Young Dong Noh [b]

[a] CAS Key Laboratory of Mineralogy and Metallogeny, Guangzhou Institute of Geochemistry, Chinese Academy of Sciences, Guangzhou 510640, PR China
[b] Materials Research Laboratory, Department of Ecosystem Science and Management and Materials Research Institute, The Pennsylvania State University, University Park, PA 16802, USA
[c] Guangdong Provincial Key Laboratory of Mineral Physics and Materials, Guangzhou 510640, PR China
[d] University of Chinese Academy of Sciences, Beijing 100049, PR China
[e] School of Chemistry and Environment, South China Normal University, Guangzhou 510006, PR China

ARTICLE INFO

Article history:
Received 18 March 2016
Received in revised form 24 May 2016
Accepted 25 May 2016
Available online 1 June 2016

Keywords:
Saponite
Broken bonds
^{29}Si MAS NMR
Q^2 environments
Silylation

ABSTRACT

A series of saponites (Sap) with a fixed Si/Mg ratio and varied Al contents were synthesized by using hydrothermal methods. The spectral, structural and morphology characters of the obtained products were characterized by a combination of XRD, FTIR, TG-DTG, TEM, ^{29}Si MAS NMR, ^{13}C NMR etc. before and after 3-aminopropyltriethoxysilane (APTES) grafting. XRD patterns showed that well-ordered Sap were obtained with starting Si/Al ratios of 5.43 and 7.89. Silylation reactions have little or no effect on the layered structure of Sap at the used dosage of APTES. The existence of the $-CH_2$ stretching bands at around 2937 cm^{-1} in IR spectra clearly showed the incorporation of silane in the grafted samples. TG–DTG curves revealed that the samples with higher crystallinity displayed higher dehydroxylation temperature, as expected. A new mass loss located at around 420 °C in silylated Sap was ascribed to the volatilization of the alkyl group in silane. The ^{29}Si NMR spectroscopy showed a series of signals of T structures, ascribed to the different silylation modes between silane and Sap. Furthermore, silylation procedures led to a decrease of the intensity of the signals at ca. −84 ppm along with an increase of the intensity of Q^3 signals. A further increase in the silane concentration did not decrease the resonance at −84 ppm any further. This phenomenon confirmed the coexistence of Q^2 structure with Q^3Si(2Al) structure, which resulted from the broken bonds at the edge surfaces of the synthesized Sap.

1. Introduction

The polarity of clay minerals is one of the key concerns during their industrial applications in clay–polymer nanocomposites (Wypych and Satyanarayana, 2005; Ha et al., 2008; Park et al., 2009), environmental materials (Tonlé et al., 2003; Sayılkan et al., 2004), drug delivery and enzyme immobilization (An et al., 2015). Ion exchange method was proven as an easily operated and efficient method to modify the surface of clay minerals and change their surface polarity to hydrophobic (de Paiva et al., 2008). However, the long alkyl chain cationic surfactant, e.g. hexadecyltrimethylammonium bromide, might leach in to the surrounding medium when organoclays are used in solutions (Waddell et al., 1981).

Silylation, also known as silane grafting, is a promising modification method, providing covalent linkages between organic components and clay mineral surface (Ruiz-Hitzky and Fripiat, 1976; Tao et al., 2011). Compared with the traditional organic cation exchange modification method, silylation method enables a durable immobilization of the reactive organic groups in the resultant products, preventing their leaching. More importantly, by introducing special functional groups (e.g. $-NH_2$, –SH), in the used silanes, the affinities and adsorption selectivity of the resultant materials to the special target molecules, such as organic and metallic contaminants, the amount of loaded enzyme and drugs etc., could be greatly improved (Ruiz-Hitzky and Fripiat, 1976; Tonlé et al., 2003; Sayılkan et al., 2004; Wypych and Satyanarayana, 2005; Ha et al., 2008; Park et al., 2009; An et al., 2015). On the other hand, these functional groups can react with the polymer matrix, resulting in the formation of a network of clay mineral, silane and polymer through covalent bonding. This can greatly improve the mechanical properties of the resulting clay-polymer nanocomposites and may lead to a breakthrough in synthesis of novel materials (Ha et al., 2008; Park et al., 2009; Wypych and Satyanarayana, 2005).

Saponite (Sap), generally presented as M_x^+ $[Si_{4-x}Al_x][Mg_3]O_{10}(OH)_2 \cdot nH_2O$ (M = Na, Li, K etc.), is a 2:1 type trioctahedral

* Corresponding authors at: CAS Key Laboratory of Mineralogy and Metallogeny, Guangzhou Institute of Geochemistry, Chinese Academy of Sciences, Guangzhou 510640, PR China, & Materials Research Laboratory, Department of Ecosystem Science and Management and Materials Research Institute, The Pennsylvania State University, University Park, PA 16802, USA.
E-mail addresses: taoqi@gig.ac.cn (Q. Tao), komarneni@psu.edu (S. Komarneni).

http://dx.doi.org/10.1016/j.clay.2016.05.026
0169-1317/

clay minerals of the smectite group. Its layer contains a central brucite-like [$Mg_3(O,OH)_6$] octahedral sheet sandwiched by two [$Si(O)_4$] tetrahedral sheets on both sides (Brigatti et al., 2006). Four out of six OH^- groups are replaced by oxygen atoms in octahedral sheet of saponite. These oxygen atoms are shared by the tetrahedral sheets. Sap has much higher surface acidity and thermal stability than its dioctahedral smectite counterpart, montmorillonite (Casagrande et al., 2005; Vogels et al., 2005). The edge surfaces of clay minerals are covered by the "undercoordinated" metal ions such as, Si^{4+}, Al^{3+}, Fe^{3+}, Mg^{2+} etc. This broken edge bond was evidenced by the adsorption of negatively charged gold colloids, as observed by Thiessen (1942) through electron microscope. However, due to the low edge surface area in the natural clay minerals such as montmorillonite, kaolinite etc., the broken bond related signal is generally absent in their ^{29}Si NMR spectra. Pioneering work by Herrera et al. (2004) showed that Sap subgroup minerals generally have a higher ratio of lateral thickness/particle diameter than montmorillonites. This kind of broken edge bonds induce Q^2 environments for the Si atoms, which can be confirmed by a ^{29}Si NMR chemical shift at ca. −85 ppm (Herrera et al., 2004; He et al., 2014). These sites readily react with silane and produce materials that are silylated on the edges (Herrera et al., 2005). Although previous studies showed the possibilities of silylation of hectorite, only limited research was focused on the silylation of Sap, which is related to silylation sites and bonding function between silane and Sap surface.

Therefore, in this study a series of Sap with a fixed Si/Mg ratio (4:3) were synthesized using hydrothermal methods, and subsequently silylated with 3-aminopropyltriethoxysilane (APTES). The structures and properties of the Sap before and after silylation were characterized by X-ray diffraction (XRD), Fourier transform infrared spectroscopy (FTIR), transmission electron microscopy (TEM), and thermogravimetric analysis (TG–DTG). The bonding modes between Sap and APTES were further determined by solid-state magic angle spinning nuclear magnetic resonance (^{29}Si MAS NMR and ^{13}C MAS NMR) spectroscopy. The new insights obtained in this study are of high importance for advancing our fundamental understanding of the mechanisms underlying the silylation of clay mineral surfaces.

1.1. Experimental methods

1.1.1. Preparation methods

1.1.1.1. Synthesis of Sap. Sap samples with a fixed Si/Mg ratio were prepared by modifying a previously reported method (Kawi and Yao, 1999; He et al., 2014). A mixture of 18.00 g of NaOH and 32.80 g of $NaHCO_3$ was dissolved in 250 mL of deionized water. Then, 38.65 g of sodium metasilicate ($Na_2SiO_3 \cdot 9H_2O$) were added under vigorous stirring (Solution A). Desired amounts of $AlCl_3 \cdot 6H_2O$ and 30.80 g of $MgCl_2 \cdot 6H_2O$ were dissolved in 25 mL of deionized water (Solution B). Solution B was slowly input into Solution A under continuous stirring to form a uniform gel. The fresh gel was then sealed into a Teflon-lined stainless steel autoclave and treated at 160 °C for 24 h. The obtained precipitates were washed by centrifuge–washing cycles until the supernatant reached neutral pH, then dried at 80 °C and ground for the further treatments. The obtained products were marked as Sap-X (X = Si/Al ratio in the starting material).

1.1.1.2. Grafting Sap with organosilane. The grafting reaction was carried out in a mixture of water/ethanol (25/75 by volume) (He et al., 2005). A mixture of 3.00 g of synthetic Sap and desired amount of APTES (99%, Aldrich) were put into 60 mL of water/ethanol and dispersed by stirring at 80 °C for 24 h. After washing by centrifuge–washing cycles using the water/ethanol solution and drying at 80 °C, the resultant products were ground and stored before characterization. The grafting products prepared from Sap-X were denoted as Sap-X-nAP, where nAP represents silylated sample synthesized using n·mmol APTES. For example, Sap-5.43-30AP represents the silylated sample of Sap-5.43 reacted with 30 mmol APTES.

1.1.2. Analytical techniques

X-ray diffraction patterns (XRD) of the samples, were collected between 1° and 80° (2θ) at a scanning rate of 1° (2θ) min^{-1} on a Bruker D8 Advance diffractometer with Ni-filtered CuKα radiation (λ = 0.154 nm, 40 kV and 40 mA).

Fourier transform infrared (FTIR) spectra were obtained using a Bruker VERTEX 70 Fourier transform infrared spectrometer. All spectra were collected at room temperature over the range of 400–4000 cm^{-1} with a resolution of 4 cm^{-1} and 64 scans.

Thermogravimetric (TG) analysis was carried out on a Netzsch STA 409 PC/PG instrument, employing a heating rate of 10 °C min^{-1} from 30 to 900 °C under a nitrogen flow of 60 mL min^{-1}.

Transmission electron microscopy (TEM) images were collected on a JEOL 2010 high resolution transmission electron microscope operated at an accelerating voltage of 200 kV. Specimens were prepared by dispersing the sample in ethanol and ultrasonically treating for 5 min. A drop of the resultant dispersion was placed on a holey carbon film supported by a copper grid, after which the ethanol was evaporated.

All the solid-state NMR experiments were carried out at $B_0 = 9.4$ T on a Bruker AVANCE III 400 WB spectrometer with an H-X BL4 double-resonance probe. The corresponding resonance frequency of ^{29}Si was 79.5 MHz. Samples were packed in a 7 mm ZrO_2 rotor and spun at the magic angle (54.7°) with the spin rate of 7 kHz. ^{29}Si MAS NMR spectra were acquired using direct excitation with ^1H high power decoupling using a 90° pulse of 6.0 μs and a recycle delay of 60 s. The ^{29}Si chemical shift was referenced to kaolinite at −91.5 ppm. The resonance frequency of ^{13}C was 100.6 MHz. Samples were packed in a 4 mm ZrO_2 rotor and spun at the magic angle (54.7°). The spin rate was 6 kHz. ^1H—^{13}C CP MAS NMR spectra were recorded with a contact time of 2.0 ms and a recycle delay of 5 s. The ^{13}C chemical shift was externally referenced to tetramethylsilane at 0 ppm.

2. Results and discussion

2.1. FTIR spectroscopy

For Sap (Fig. 1a), the –OH stretching bands were at around 3691 cm^{-1} (narrow and sharp, structural –OH) and 3600–3448 cm^{-1} (–OH in water). The band corresponding to the water bending mode was observed at 1642 cm^{-1}. The strong and broad band at around 1000 cm^{-1} is due to the stretching mode Si—O—Si. The bands in the region of 430–460 cm^{-1} were attributed to deformation vibrations of Si—O—Mg. These bands were very similar with those for natural montmorillonite (Fig. 1) (Xue et al., 2007).

The bands in the range of 457–467 cm^{-1} were used to distinguish the smectites between di- and trioctahedral structures. Because Mg^{2+} has higher electronegativity than Al^{3+}, the location for the deformation vibration region of Si—O—Mg in Sap (457–465 cm^{-1}) is generally lower than that of Si—O—Al in montmorillonite (above 467 cm^{-1}). In dioctahedral montmorillonite, this band might split, due to the differences in nearest neighbor environment of the octahedral Al^{3+} such as the number of vacancies (Yao et al., 2005). In the present samples, all such deformation vibrations located in the region of 452–463 cm^{-1} did not show any splitting (Fig. 1). This strongly suggests that all these synthetic Sap are of trioctahedral structure. The most intense Si—O—Si stretching vibrations were observed in the Sap products Sap-5.43 (Fig. 1c) and Sap-7.89 (Fig. 1e), which suggested that these samples are of higher crystallinity than the other samples in this study.

Generally, four main changes are expected in the IR spectra of silylated products corresponding to the stretching vibrations of the surface –OH, surface water, the alkyl chain and Si—O vibrations (Figs. 1b, d and e) (Herrera et al., 2005). First, the shape and width of the Si—O stretching related absorptions were changed in the region of 1000–

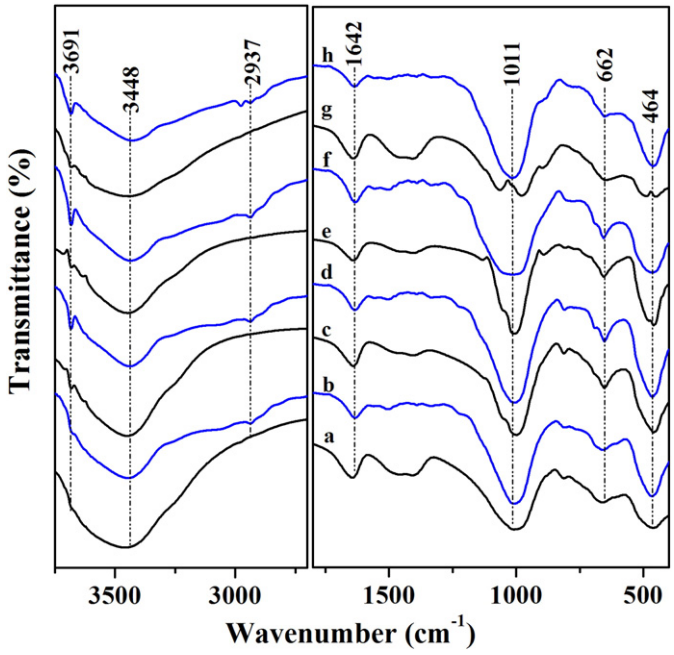

Fig. 1. The FTIR spectra of the Sap and their silylated products. a. Sap-2.33; b. Sap-2.33-30AP; c. Sap-5.43; d. Sap-5.43-30AP; e. Sap-7.89; f. Sap-7.89-30AP; g. Sap-12.3; h. Sap-12.3-30AP.

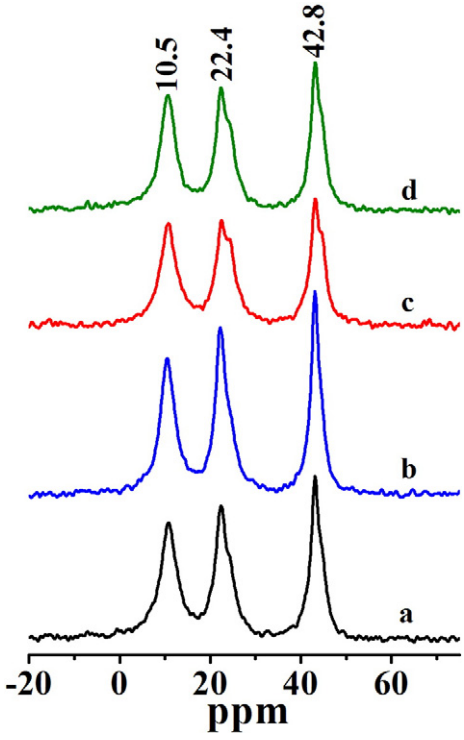

Fig. 2. The ^{13}C MAS NMR spectra Sap silylated with different concentration of APTES. a. Sap-2.33-30AP; b. Sap-5.43-30AP; c. Sap-7.89-30AP; d. Sap-12.3-30AP.

1200 cm^{-1}. (Culler et al., 1983; Mackenzie, 1994). Silane related change was the appearance of $-CH_2$ stretching (region 2980–2800 cm^{-1}) together with very weak signals at around 1520 cm^{-1}, corresponding to $-NH_2$ deformation (Fig. 1). Important evidence was also observed in the region associated with –OH stretching related modes. The broad and small band between 3700 and 3300 cm^{-1} was replaced by much lower intensity bands. This indicated that the silylated products have higher hydrophobicity than Sap. Also it may be contributed partly from the incomplete condensation of silane. In addition, the Mg—OH bands at 3691 cm^{-1} were intensified, which may also have resulted from the reduction of surface water. All these changes in FTIR spectra suggest that APTES was successfully grafted on Sap.

2.2. ^{13}C CP MAS NMR spectroscopy

There are usually five chemical shifts in the ^{13}C NMR spectra of APTES ($H_2N—CH_2(3)–CH_2(2)–CH_2(1)-Si(–O—CH_2(4)–CH_3(5))_3$), i.e. 59 (C5), 46 (C3), 28 (C2), 19 (C4), and 8.6 (C1) ppm (Kallury et al., 1994; Kim et al., 2011). The silylated Sap showed signals at 10.5, 22.4, and 42.8 ppm, corresponding to C1, C2 and C3, respectively (Fig. 2). The existence of these signals with the change in chemical shifts proved the successful grafting of silane onto the surface of Sap (Kallury et al., 1994). The absence of the signals of methylene (C5, 59 ppm) and methyl groups (C4, 19 ppm) in ethoxyl groups connected to silicon atom, respectively, implies the complete hydrolysis of the ethoxyl groups and/or the combination of hydrolysis and grafting processes (Fig. 2). The broadening of the C2 peak at 22.4 ppm suggests the presence of a small fraction of protonated amine groups (Kallury et al., 1994).

2.3. X-ray diffraction (XRD) patterns

The powder XRD patterns of the synthetic samples showed a series of reflections at ca. 2.8, 19.4, 34.2, and 60.3° 2 theta degrees, which are attributed to (001), (02,11), (13,20), and (060) reflections of the synthetic products, respectively (Fig. 3) (Vogels et al., 2005; He et al., 2014). The d values of (001) reflections at ca. 1.33–1.41 nm were typical values of the Na-Sap. The d values of (006) reflections were ca. 0.153 nm, confirming that the Sap were of a trioctahedral nature of clay mineral structures (Grauby et al., 1993). There were no obvious reflections of any impurities, indicating that pure Sap had been successfully synthesized (Fig. 3). Compared to natural Sap, the synthetic samples displayed broader and weaker (001) reflections. This suggested that the crystallinity of the synthetic Sap is relatively poor. However, relatively strong (001) reflections were recorded for Sap-5.43 and Sap-7.89 (Fig. 3) in this study, indicating that well-crystallized and ordered Sap were formed with the Si/Mg ratios of 5.43 and 7.89 as has been suggested

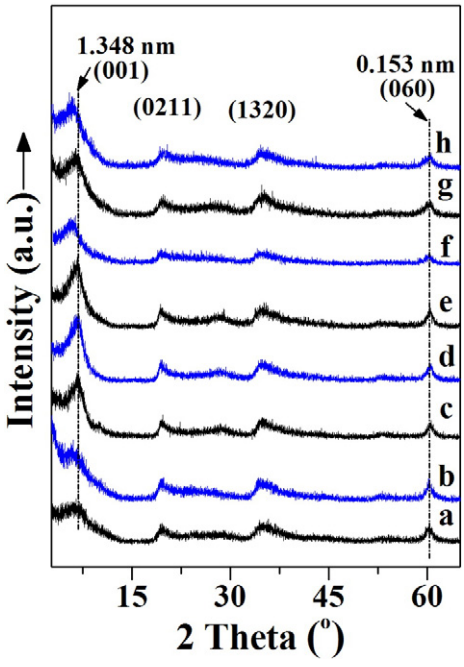

Fig. 3. The XRD patterns of the Sap and their silylated products. a. Sap-2.33; b. Sap-2.33-30AP; c. Sap-5.43; d. Sap-5.43-30AP; e. Sap-7.89; f. Sap-7.89-30AP; g. Sap-12.3; h. Sap-12.3-30AP.

by IR spectra (vide supra). With an increase or decrease of Si/Al ratio, the (001) reflection was obviously weakened and broadened, corresponding to poorly crystallized synthetic Sap. Therefore, it can be concluded that the initial Si/Al ratio has a prominent effect on the crystallinity of the synthetic Sap (He et al., 2014).

The silylation processes had little influence on the structure of the final products. The minor increases in the d values might be due to the partial intercalation of APTES, which is a very common phenomenon in silylated and surfactant modified layered minerals (Tao et al., 2011). It may also indicate that the silane molecules were mainly hydrolyzed with moisture and condensed with the hydroxyl groups on the external surface and/or edges of Sap.

2.4. Thermal analysis

Typically, three mass losses can be observed in TG curves for the thermal decomposition of Sap (Fig. 4a). A big and broad endotherm at around 110 °C is attributed to the loss of adsorbed and interlayer water. Following this, a mass loss may occur in the region of 300–600 °C, ascribed to the loss of strongly held interlayer water and some hydroxyls. The mass loss ends with a dehydroxylation process at above 700 °C. The previous researches showed that the dehydroxylation temperature of Sap was closely connected with its crystallinity (Zhang et al., 2016) and the composition in its layer (Vogels et al., 2005). For the samples with Si/Al ratios of 5.43 and 7.89, the dehydroxylation temperatures were over 760 °C. When Si/Al increased to 12.3 or decreased to 2.33, the temperature dropped down to 748 °C or 716 °C, respectively. The dehydroxylation temperature was related to the crystallinity as deduced from the FTIR and XRD results.

The silylation procedures brought three main differences as displayed in the TG–DTG curves of the products (Fig. 4). First, the surface and interlayer water desorption temperature decreased by ca. 10 °C along with the mass losses reduced by half compared to those of the Sap, which were not silylated. These results imply a decrease in hydrophilicity of the samples. These results are supported by the data from the FTIR spectra, which showed width and intensity variations in water related –OH stretching vibrations (vide supra). Another important change was that a new mass loss of around 8–12% in the region of 250–600 °C occurred for the silylated products, which can be attributed to the alkyl chain decomposition/volatilization of the grafted silanes. TG–DTG curves also showed that the silylated samples with higher Si/Al ratio exhibited lower total mass loss compared to the silylated Sap with lower Si/Al ratio. This may be due to the higher crystallinity of the Sap with higher Si/Al ratio as they contained fewer edge hydroxyl groups, which are needed for silane grafting.

3. TEM images

TEM photographs of the samples showed typical clay mineral platelets, which are aggregated. There was no obvious gradual change of morphology with an increase of Si/Al ratio (Fig. 5). After silylation, the Sap crystals tend to bond with one another to form stacked particles with the fluffy structures. As APTES has three siloxane bonds, they can condense with each other as well as with the surface hydroxyl groups of Sap. This leads to the formation of the Si—O—Si linkage matrix among two or more adjacent fine Sap particles (Tao et al., 2011).

3.1. ^{29}Si MAS NMR spectroscopy

To better understand the bonding formed between Sap and silane, ^{29}Si MAS NMR was used to assess the nearest neighbor environment of Si in Sap and their silylated products (Fig. 6). $Q^m(nAl)$ (m = 0, 1, 2, 3 and 4) and T^n (n = 0, 1, 2 and 3) were adopted to describe the Si environments in the solid products, in which, Q^m and T^n refer to the polymerization state of Si, and nAl ($n = 0, 1\ldots$ m-1) refers to the number of Al in the next-nearest neighbor tetrahedral position, and n to the number of "O bridge" structures formed between APTES and the Sap or the neighboring APTES, respectively (Lipsicas et al., 1984).

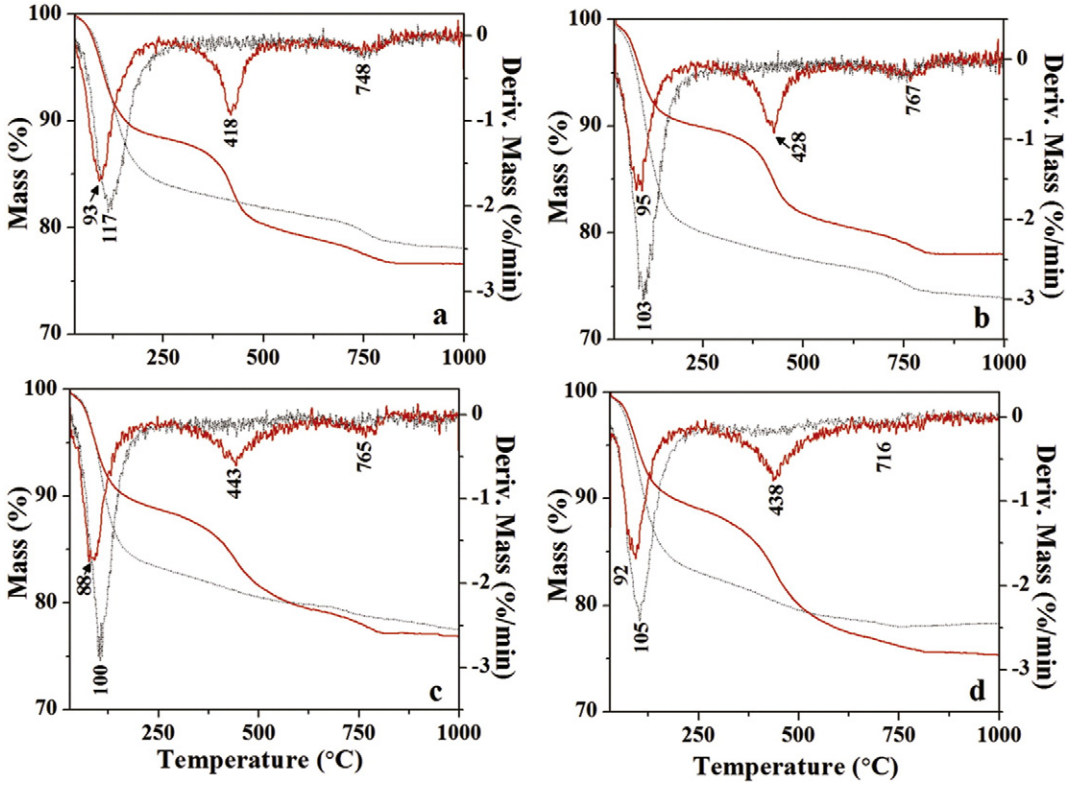

Fig. 4. TG–DTG curves of the Sap (dotted lines) and their silylated products (solid lines). a. Sap-2.33 and Sap-2.33-30AP; b. Sap-5.43 and Sap-5.43-30AP; c. Sap-7.89 and Sap-7.89-30AP; d. Sap-12.3 and Sap-12.3-30AP.

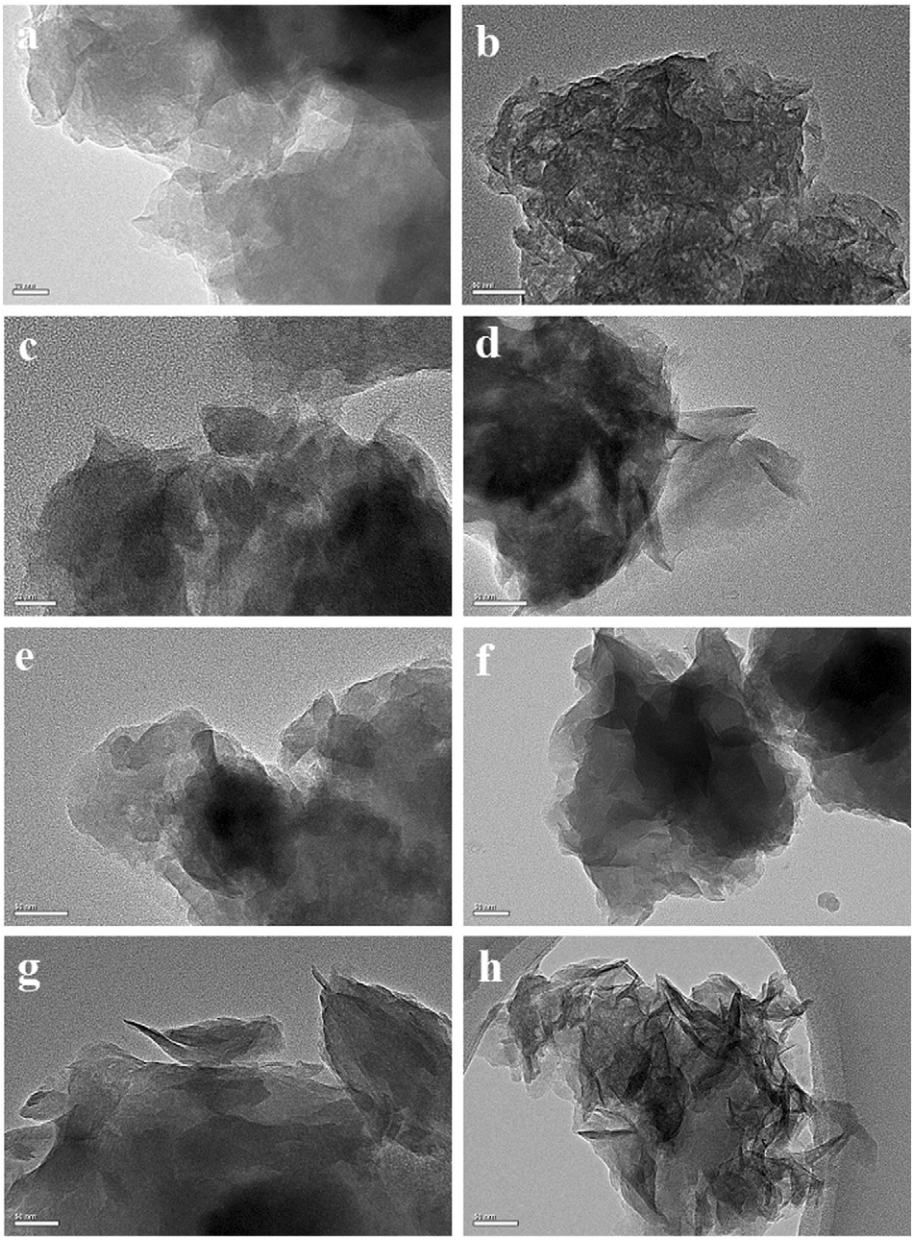

Fig. 5. TEM images of Sap and the related silylated products. a. Sap-2.33; b. Sap-2.33-30AP; c. Sap-5.43; d. Sap-5.43-30AP; e. Sap-7.89; f. Sap-7.89-30AP; g. Sap-12.3; h. Sap-12.3-30AP.

For the as-synthesized Sap, three types of ^{29}Si signals were found, which were located at approximately −95, −91 and −83.8 ppm (Fig. 6). Among them, the former two were of high intensity, which were attributed to Q^3 Si(0Al) and Q^3 Si(1Al), respectively. The Sap-2.33 sample, which contained maximum amounts of both tetrahedral and octahedral Al showed maximum intensity for Q^3 Si(1Al) resonance but lower intensity for Q^3 Si(0Al) resonance. With decreasing Al content, the intensity of Q^3 Si(0Al) resonance increased while the intensity of Q^3 Si(1Al) resonance decreased (Fig. 6). The resonance at −83.8 ppm can be attributed to either Q^3 Si(2Al) (Lipsicas et al., 1984; Delevoye et al., 2003) environment or to the Q^2 Si(OAl) environment at the layer edges of clay minerals (Vogels et al., 2005) or both. The intensity of the resonance at −83.8 ppm decreased with decreasing Si/Al ratio (Fig. 6, dotted lines). However, the intensity of these resonances at −83.8 ppm clearly decreased in the silylated samples but they did not disappear. These results confirmed the existence of Q^2 Si(OAl) as well as a small amount of Q^3 Si(2Al). In order to further prove that the resonance was composed of a small amount of Q^3 Si(2Al), additional experiments were done using larger amounts of silane. The larger amounts of silane did not decrease the resonance at −83.8 ppm any further i.e., this resonance did not disappear after grafting reaction with enough concentration of silanes (Fig. 7), which may imply the coexistence of Q^3 Si(2Al) resonance along with Q^2 Si(OAl). Thus both these environments were indicated by the ^{29}Si MAS NMR resonance at −83.8 ppm (Figs. 6 and 7).

There were also three obvious signals centered at −53.7, −58.5 and −67.5 ppm for the silylated products, ascribed to the T^1, T^2 and T^3 bonding modes, respectively (Tao et al., 2011). The presence of the signal at −58.5 ppm can be explained by the even dispersion of APTES of a relatively lower concentration, whose molecules probably existed without any condensation with one another, resulting in a higher population of T^1 structure in the products. The increases of the concentration of APTES led mainly to the increase of the T^3 bonding modes and decrease of T^1 bonding modes (Fig. 7). This resulted in more condensation among the silane molecules. All the intensities of the Q signals remained with the increase of silane concentration over 30 mmol, which suggested that the grafting process did not influence the layer microstructure of Sap even when the concentration of silane reached a certain high level.

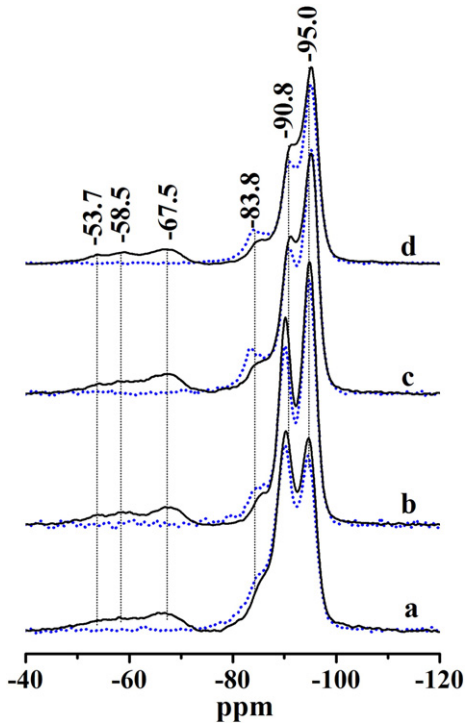

Fig. 6. The ^{29}Si MAS NMR spectra of Sap before (dotted line) and after (solid line) silylation. a. Sap-2.33 and Sap-2.33-30AP; b. Sap-5.43 and Sap-5.43-30AP; c. Sap-7.89 and Sap-7.89-30AP; d. Sap-12.3 and Sap-12.3-30AP.

4. Conclusions

A series of Sap with the fixed Si/Mg ratio was successfully synthesized using hydrothermal method. FTIR spectra revealed that all the products were of trioctahedral smectite structure, as shown by Si—O—Mg deformation vibrations of Sap (457–465 cm^{-1}). The d(060) values were around 0.153 nm as determined by XRD, which suggested trioctahedral structure. Both FTIR and XRD confirmed that the Sap with the Si/Al ratios of 5.43 and 7.89 were of the highest crystallinity. TG-DTG curves showed that the Sap with higher crystallnities exhibited higher hydroxylation temperatures (over 760 °C). The ^{29}Si MAS NMR spectra indicated that the silylation mode was mainly with T^3 structures and increasing the silane content led to an increase in the amount of T^3 structures and the absence of T^1 structure. The ^{29}Si resonance at ca. −84 ppm was attributed to both Q^2 Si(OAl) and Q^3 Si(2Al) environments through grafting of APTES.

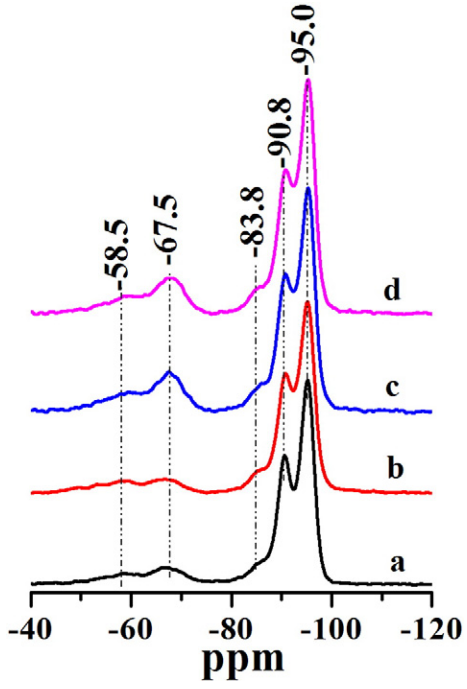

Fig. 7. The ^{29}Si MAS NMR spectra of Sap silylated with different concentration of APTES. a. Sap-5.43-15AP; b. Sap-5.43-30AP; c. Sap-5.43-60AP; d. Sap-5.43-100AP.

Acknowledgments

The financial supports of the National Natural Science Foundation of China (Grant no. 41372048, and 41530313) and the CAS/SAFEA International Partnership Program for Creative Research Teams (Grant No. 20140491534) were acknowledged. Q. Tao is grateful to The China Scholarship Council (CSC) for the overseas funding (File No. 201504910225) to visit The Pennsylvania State University.

References

An, N., Zhou, C.H., Zhuang, X.Y., Tong, D.S., Yu, W.H., 2015. Immobilization of enzymes on clay minerals for biocatalysts and biosensors. Appl. Clay Sci. 114, 283–296.
Brigatti, M.F., Galan, E., Theng, B.K.G., 2006. Structures and mineralogy of clay minerals. In: Bergaya, F., Theng, B.K.G., Lagaly, G. (Eds.), Handbook of Clay Science. Elsevier, Amsterdam, pp. 19–86.
Casagrande, M., Storaro, L., Lenarda, M., Rossini, S., 2005. Solid acid catalysts from clays: oligomerization of 1-pentene on Al-pillared smectites. Catal. Commun. 6, 568–572.
Culler, S.R., Naviroj, S., Ishida, H., Koenig, J.L., 1983. Analytical and spectroscopic investigation of the interaction of CO_2 with amine functional silane coupling agents on glass fibers. J. Colloid Interface Sci. 96, 69–79.
de Paiva, L.B., Morales, A.R., Valenzuela Díaz, F.R., 2008. Organoclays: properties, preparation and applications. Appl. Clay Sci. 42, 8–24.
Delevoye, L., Robert, J.L., Grandjean, J., 2003. ^{23}Na 2D 3QMAS NMR and ^{29}Si, ^{27}Al MAS NMR investigation of laponite and synthetic saponites of variable interlayer charge. Clay Miner. 38, 63–69.
Grauby, O., Petit, S., Decarreau, A., Baronnet, A., 1993. The beidellite-saponite series — an experimental approach. Eur. J. Mineral. 5, 623–635.
Ha, S.R., Rhee, K.Y., Kim, H.C., Kim, J.T., 2008. Fracture performance of clay/epoxy nanocomposites with clay surface-modified using 3-aminopropyltriethoxysilane. Colloids Surf. A Physicochem. Eng. Asp. 313–314, 112–115.
He, H.P., Duchet, J., Galy, J., Gerard, J., 2005. Grafting of swelling clay minerals with 3-aminopropyltriethoxysilane. J. Colloid Interface Sci. 288, 171–176.
He, H.P., Li, T., Tao, Q., Chen, T.H., Zhang, D., Zhu, J.X., Yuan, P., Zhu, R.L., 2014. Aluminum ion occupancy in the structure of synthetic saponites: effect on crystallinity. Am. Mineral. 99, 109–116.
Herrera, N.N., Letoffe, J.M., Putaux, J.L., David, L., Bourgeat-Lami, E., 2004. Aqueous dispersions of silane-functionalized laponite clay platelets. A first step toward the elaboration of water-based polymer/clay nanocomposites. Langmuir 20, 1564–1571.
Herrera, N.N., Letoffe, J.M., Reymond, J.-P., Bourgeat-Lami, E., 2005. Silylation of laponite clay particles with monofunctional and trifunctional vinyl alkoxysilanes. J. Mater. Chem. 15, 863–871.
Kallury, K.M.R., Macdonald, P.M., Thompson, M., 1994. Effect of surface-water and base catalysis on the silanization of silica by (aminopropyl)alkoxysilanes studied by X-ray photoelectron-spectroscopy and ^{13}C cross-polarization magic-angle-spinning nuclear-magnetic-resonance. Langmuir 10, 492–499.
Kawi, S., Yao, Y.Z., 1999. Saponite catalysts with systematically varied Mg/Ni ratio: synthesis, characterization, and catalysis. Microporous Mesoporous Mater. 33, 49–59.
Kim, S.H., Han, O.H., Kim, J.K., Lee, K.H., 2011. Multinuclear solid-state NMR investigation of nanoporous silica prepared by sol-gel polymerization using sodium silicate. Bull. Kor. Chem. Soc. 32, 3644–3649.
Lipsicas, M., Raythatha, R.H., Pinnavaia, T.J., Johnson, I.D., Giese Jr., R.F., Costanzo, P.M., Robert, J.-L., 1984. Silicon and aluminium site distributions in 2:1 layered silicate clays. Nature 309, 604–607.
Mackenzie, J.D., 1994. Structures and properties of ormosils. J. Sol-Gel Sci. Technol. 2, 81–86.
Park, S.-J., Kim, B.-J., Seo, D.-I., Rhee, K.-Y., Lyu, Y.-Y., 2009. Effects of a silane treatment on the mechanical interfacial properties of montmorillonite/epoxy nanocomposites. Mater. Sci. Eng. A 526, 74–78.
Ruiz-Hitzky, E., Fripiat, J.J., 1976. Organomineral derivatives obtained by reacting organochlorosilanes with the surface of silicates in organic solvents. Clay Clay Miner. 24, 25–30.
Sayılkan, H., Erdemoğlu, S., Şener, Ş., Sayılkan, F., Akarsu, M., Erdemoğlu, M., 2004. Surface modification of pyrophyllite with amino silane coupling agent for the removal of 4-nitrophenol from aqueous solutions. J. Colloid Interface Sci. 275, 530–538.
Tao, Q., Zhu, J.X., Wellard, R.M., Bostrom, T.E., Frost, R.L., Yuan, P., He, H.P., 2011. Silylation of layered double hydroxides via an induced hydrolysis method. J. Mater. Chem. 21, 10711–10719.
Thiessen, P.A., 1942. Wechselseitige adsorption von Kolloiden. Z. Elektrochem. Angew. Phys. Chem. 48, 675–681.

Tonlé, I.K., Ngameni, E., Njopwouo, D., Carteret, C., Walcarius, A., 2003. Functionalization of natural smectite-type clays by grafting with organosilanes: physico-chemical characterization and application to mercury(II) uptake. Phys. Chem. Chem. Phys. 5, 4951–4961.

Vogels, R., Kloprogge, V.T., Geus, J.W., 2005. Synthesis and characterization of saponite clays. Am. Mineral. 90, 931–944.

Waddell, T.G., Leyden, D.E., DeBello, M.T., 1981. The nature of organosilane to silica-surface bonding. J. Am. Chem. Soc. 103, 5303–5307.

Wypych, F., Satyanarayana, K.G., 2005. Functionalization of single layers and nanofibers: a new strategy to produce polymer nanocomposites with optimized properties. J. Colloid Interface Sci. 285, 532–543.

Xue, W.H., He, H.P., Zhu, J.X., Yuan, P., 2007. FTIR investigation of CTAB–Al–montmorillonite complexes. Spectrochim. Acta Part A 67, 1030–1036.

Yao, M., Liu, Z., Wang, K., Zhu, M., Sun, H., 2005. Application of FTIR technique in microwave-hydrothermal synthesis of saponite. Spectrosc. Spectr. Anal. 25, 870–873.

Zhang, D., He, H.P., Tao, Q., Chen, M.Y., Ji, S.C., Li, T., 2016. Heterogeneous hydrothermal synthesis of saponite and the factors affect its crystallinity. Acta Mineral. Sin. 36, 235–240.